Region Based Image Segmentation using a Modified Mumford-Shah Algorithm

Jung-ha An[1] and Yunmei Chen[2]

[1] Institute for Mathematics and its Applications (IMA), University of Minnesota, USA,
[2] Department of Mathematics, University of Florida, USA.

Abstract. The goal of this paper is to develop region based image segmentation algorithms. Two new variational PDE image segmentation models are proposed. The first model is obtained by minimizing an energy function which depends on a modified Mumford-Shah algorithm. The second model is acquired by utilizing prior shape information and region intensity values. The numerical experiments of the proposed models are tested against synthetic data and simulated normal human-brain MR images. The preliminary experimental results show the effectiveness and robustness of presented models against to noise, artifact, and loss of information.

1 Introduction

Segmentation techniques have been developed to capture the object boundary by several different approaches; edge-based methods mainly using active contour models, region-based methods, or the combination of the two by using Geodesic Active Region models.

The most celebrating region based image segmentation model is introduced by Mumford and Shah in 1989 [15]. In this model, an image is decomposed into a set of regions within the bounded open set Ω and these regions are separated by smooth edges Γ. Ambrosio and Tortorelli approximated the measurement of an edge Γ length term in the Mumford-Shah model by a quadratic integral of an edge signature function in 1990 [1]. Chan and Vese proposed a piecewise constant Mumford-Shah model in [4, 5] by using a level set formulation [16]. Developments of variational level set implementation techniques based Mumford-Shah model are followed by [8, 9, 13]. The segmentation is represented by characteristics functions using phase fields in [8, 13]. The details of phase field theory can be found in [2, 14, 18–20].

Recently, a soft (fuzzy) Mumford-Shah segmentation of mixture image patterns is introduced by [19]. This technique is defined by using the Bayesian rationale and the MAP estimator. It has been shown that hard segmentation technique is the special case of soft segmentation in [19]. The first proposed model in this paper is motivated by [8, 18, 19]. The region based variational partial differential equation (PDE) image segmentation model is suggested. The model is obtained by minimizing an energy function which depends on a modified Mumford-Shah algorithm. A fuzzy segmentation in our model is similar to Shen [18, 19], but our model is variational which differs from Esedoglu [8].

Yet these algorithms have a limit to obtain an efficient segmentation result, if images have strong noise, occlusion, or loss of information. The prior shape information has

been incorporated into the segmentation process to overcome these problems [3, 6, 7, 10–12, 17]. The second suggested model in this paper is acquired by using prior shape information and region intensity values. The prior shape information is attained by using a modified Mumford-Shah model.

Two new region based variational partial differential equation (PDE) models for an image segmentation are presented with an application to synthetic data and simulated human brain MR images. This paper is organized as follows: In section 2, a modified Mumford-Shah model is described. Euler-Lagrange equations of the suggested model are presented in this section as well. Experimental results of the model which were applied to synthetic data and simulated human brain MR images are shown. In section 3, the prior shape information based image segmentation technique is presented. Numerical results to the noisy synthetic data is also shown in this section. Finally, in section 4, the conclusion follows and future work is stated.

2 A Modified Mumford-Shah Model Based Image Segmentation

In this section, a region based image segmentation is introduced. The segmentation is attained by using a modified Mumford-Shah segmentation technique. Two phases are assumed for the simplicity of the problem in our model. The presented model is followed in a similar way from [18] with $z(\bar{x}) = \frac{2}{\pi} arctan(\frac{\bar{x}}{\epsilon})$. The model is aimed to find θ, c_1, and c_2 by minimizing the energy functional:

$$E(\theta, c_1, c_2) =$$

$$\lambda_1 \int_\Omega \{\frac{1}{2}(1 + \frac{2}{\pi}\arctan(\frac{\theta}{\epsilon}))\}^2 (I(\bar{x}) - c_1)^2 + \{\frac{1}{2}(1 - \frac{2}{\pi}\arctan(\frac{\theta}{\epsilon})\}^2$$

$$(I(\bar{x}) - c_2)^2 d\bar{x} + \lambda_2 \int_\Omega \frac{9\epsilon_1 |\nabla(\frac{\theta}{\epsilon})|^2}{\pi^2(1 + (\frac{\theta}{\epsilon})^2)^2} + \frac{(\pi^2 - 4\arctan^2(\frac{\theta}{\epsilon}))^2}{64\epsilon_1\pi^4} d\bar{x}, \qquad (2.1)$$

where I is a given image, Ω is domain, ϵ and ϵ_1 are positive parameters, and $\lambda_i > 0, \;\; i = 1, 2$ are parameters balancing the influences from the two terms in the model. Here, $c_1(\theta)$=average(I) in $\{\theta \geq 0\}$ and $c_2(\theta)$=average(I) in $\{\theta < 0\}$. As $\epsilon \to 0$, the approximation $H_\epsilon(\theta) = \frac{1}{2}(1 + \frac{2}{\pi}\arctan(\frac{\theta}{\epsilon}))$ converges to the heaviside function $H(\theta) = 1, \;\; if \; \theta \geq 0$ and $H(\theta) = 0, \;\; if \; \theta < 0$ as in [4]. The square of H_ϵ is used in our model for the computational stability. In the second term of Equation (2.1), $\epsilon_1 \ll 1$ controls the transition bandwidth. As $\epsilon_1 \to 0$, the first term is to penalize unnecessary interfaces and the second term forces the stable solution of $z(\theta)$ to take one of the two phase field values 1 or -1 in a similar way from [18]. The proposed model is similar to [4], but is different by using the Γ approximation to the piecewise-constant Mumford-Shah model.

The first term forces $\{\frac{1}{2}(1 + \frac{2}{\pi}\arctan(\frac{\theta}{\epsilon}))\}^2$, towards 0 if $I(\bar{x})$ is different from c_1 and towards 1 if $I(\bar{x})$ is close to c_1, for every $\bar{x} \in \Omega$. In a similar way, $\{\frac{1}{2}(1 - \frac{2}{\pi}\arctan(\frac{\theta}{\epsilon}))\}^2$, towards 0 if $I(\bar{x})$ is different from c_2 and towards 1 if $I(\bar{x})$ is close to c_2, for every $\bar{x} \in \Omega$.

In the theory of Γ-convergence, the measuring an edge Γ length term in the Mumford-Shah model can be approximated by a quadratic integral of an edge signature function $p(x)$ such that

$$\int_{\Gamma} dS = \int_{\Omega} (\epsilon |\nabla p|^2 + \frac{(p-1)^2}{4\epsilon}) d\bar{x}, \epsilon \ll 1$$

by Ambrosio and Tortorelli in 1990 [1]. This model is combined with double-well potential function $W(p) = p^2(1-p)^2$ which is quadratic around its minima and is growing faster than linearly at infinity, where $p \in H^1(\Omega)$. In [18], the following is suggested for two phase model:

$$\int_{\Omega} (9\epsilon |\nabla p|^2 + \frac{(1-p^2)^2}{64\epsilon}) d\bar{x},$$

where the range of p is restricted within $[-1, 1]$. Here $\epsilon \ll 1$ controls the transition bandwidth. As $\epsilon \to 0$, the first term is to penalize unnecessary interfaces and the second term forces the stable solution to take one of the two phase field values 1 or -1. The second term in our model is followed from [18]. For the details of phase field models and double-well potential functions, please refer [18–20].

2.1 Euler-Lagrange Equations of the Model

The evolution equations associated with the Euler-Lagrange equations in Equation (2.1) are

$$\begin{aligned}
\frac{\partial \theta}{\partial t} = & -\lambda_1 \{ (1 + \frac{2}{\pi} \arctan(\frac{\theta}{\epsilon})) (\frac{\epsilon^2}{\pi(\epsilon^2 + \theta^2)}) (I(\bar{x}) - c_1)^2 \\
& -(1 - \frac{2}{\pi} \arctan(\frac{\theta}{\epsilon})) (\frac{\epsilon^2}{\pi(\epsilon^2 + \theta^2)}) (I(\bar{x}) - c_2)^2 \} \\
& +\lambda_2 \{ \frac{72\epsilon_1}{\pi^2} (div(\frac{\nabla \theta}{(1+\theta^2)^2}) + \frac{2\theta |\nabla \theta|^2}{(1+\theta^2)^3}) \\
& +\frac{(\pi^2 - 4 \arctan^2(\frac{\theta}{\epsilon})) \arctan(\frac{\theta}{\epsilon})}{4\epsilon_1 \pi^4 (1 + (\frac{\theta}{\epsilon})^2)} \}, \quad in \ \Omega \\
& \frac{\partial \theta}{\partial n} = 0, \quad on \ \partial\Omega, \qquad (2.2)
\end{aligned}$$

where the optimal means c_1 and c_2 are attained by

$$c_1 = \frac{\int_{\Omega} \{ \frac{1}{2} (1 + \frac{2}{\pi} \arctan(\frac{\theta}{\epsilon})) \}^2 I(\bar{x}) d\bar{x}}{\int_{\Omega} \{ \frac{1}{2} (1 + \frac{2}{\pi} \arctan(\frac{\theta}{\epsilon})) \}^2 d\bar{x}}, \qquad (2.3)$$

$$c_2 = \frac{\int_{\Omega} \{ \frac{1}{2} (1 - \frac{2}{\pi} \arctan(\frac{\theta}{\epsilon})) \}^2 I(\bar{x}) d\bar{x}}{\int_{\Omega} \{ \frac{1}{2} (1 - \frac{2}{\pi} \arctan(\frac{\theta}{\epsilon})) \}^2 d\bar{x}}. \qquad (2.4)$$

2.2 Numerical Results

In this part, the numerical results with applications to synthetic data and simulated normal human brain MR images. The Equation (2.1) was solved by finding a steady state solution of the evolution equations. The evolution equations are associated with the Euler-Lagrange equations of the Equation (2.1). A finite difference scheme and the gradient descent method is applied to discretize the evolving equations.

The Figure 1 showed the proposed model segmentation results to synthetic data. Figure 2 showed the segmentation results by [4]. The first figure in Figure 1 and Figure 2 is the given synthetic image I with an initial contour as a solid line. In Figure 1 and Figure 2, the second image is the segmented image and the third one is the segmented contour as a solid line with I. Our model performs better than [4] to capture the boundary of the region which has similar intensity. The numerical results with an application to the simulated human brain MR image are shown from Figure 3 to Figure 6. The data is obtained from *http://www.bic.mni.mcgill.ca/brainweb*. The simulated normal human brain image with the ground truth white matter image is shown in Figure 3. In Figure 3, the first figure is the simulated brain image I, the second one is an image I with an initial contour as a solid line, and the third one is the ground truth brain white matter. From Figure 4 to Figure 5, the first image is the given image I with an initial contour as a solid line, the second image is the segmented image results by our proposed model and [4] each, and the third figure is the segmented contour in I. The numerical results of segmented image by the proposed model and [4] compared to the ground truth white matter brain image which is in the first figure are in Figure 6. Our proposed model captures the boundary of the brain image better than [4]. The second image in Figure 1, Figure2, Figure 4, and Figure 5 is obtained by $sign(\theta)$, where $sign(\theta) = 1, if \ \ \theta \geq 0$ and $sign(\theta) = -1, if \ \ \theta < 0$.

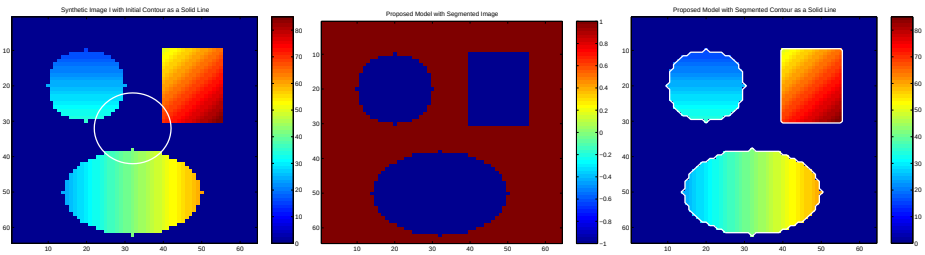

Fig. 1. Left : A Given Image I with an Initial Contour, Middle : Segmented Synthetic Image using the Proposed Model, Right : Segmented Synthetic Image with a Segmented Contour as a Solid Line

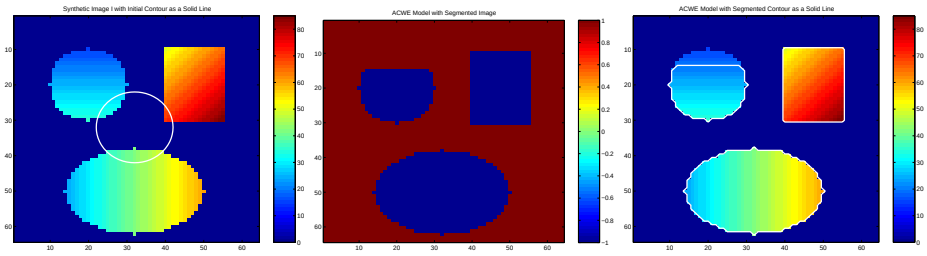

Fig. 2. Left : A Given Image I with an Initial Contour, Middle : Segmented Synthetic Image using Active Contour Without Edges Model, Right : Segmented Synthetic Image with a Contour as a Solid Line

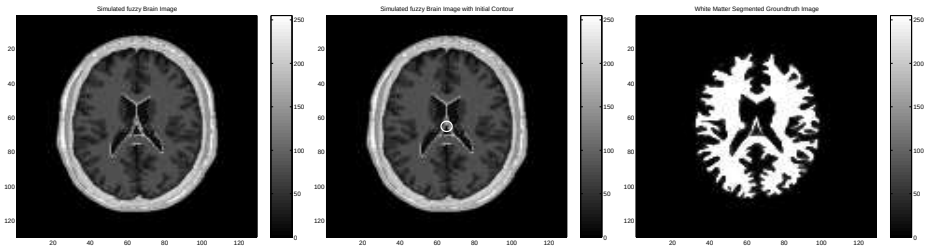

Fig. 3. Left : A Given Image I, Middle : Brain Image with an Initial Contour, Right : Ground Truth Brain White Matter

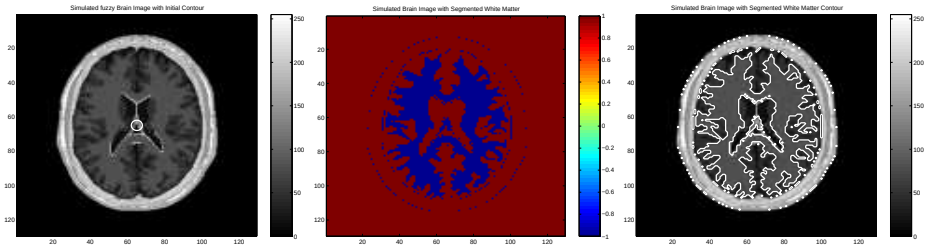

Fig. 4. Left : Brain Image with an Initial Contour, Middle : Segmented Simulated White Matter Brain Image using the Proposed Model, Right : Segmented Simulated Brain Image with a Solid Line

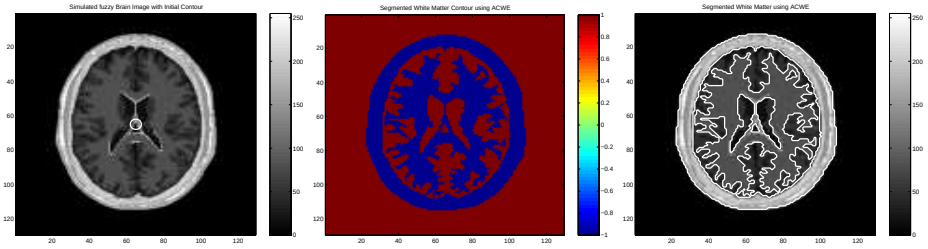

Fig. 5. Left : Brain Image with an Initial Contour, Middle : Segmented Simulated White Matter Brain Image using a Active Contour Without Edges Model, Right : Segmented Simulated Brain Image with a Solid Line

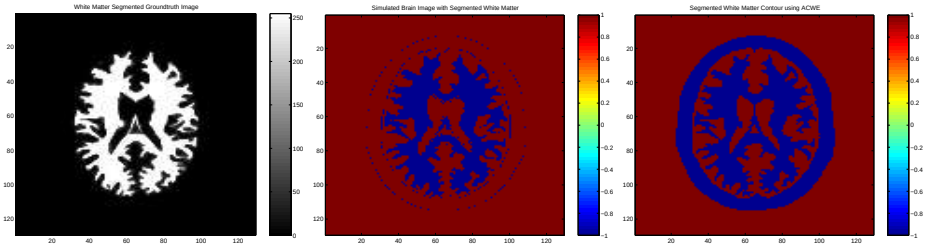

Fig. 6. Left : Ground Truth Brain White Matter Segmented Image, Middle : Segmented Simulated White Matter Brain Image by our Proposed Model, Right : Segmented Simulated White Matter Brain Image using an Active Contour without Edges Model

3 Image Segmentation using a Prior Shape Information

A new variational image segmentation model based on the region intensity information utilizing prior shape knowledge is suggested. The goal of the model is to develop the prior shape information based image segmentation technique. The shape prior is obtained by using a modified Mumford-Shah segmentation technique from section 2. Then the heaviside function was applied to θ to get binary image, where $H(\theta) = 1,\ if\ \theta \geq 0$ and $H(\theta) = 0,\ if\ \theta < 0$. In a similar way from Section 2, two phases are assumed for the simplicity of the problem in our model.

Let S be a given binary image, called shape prior information. I ia a given image and Υ is a registration mapping either a rigid transformation or nonrigid deformation. The model is aimed to find Υ, d_1, and d_2 by minimizing the energy functional:

$$E(\Upsilon, d_1, d_2) =$$
$$\int_\Omega S(\bar{x})(I(\Upsilon(\bar{x})) - d_1)^2 d\bar{x} + \lambda \int_\Omega (1 - S(\bar{x}))(I(\Upsilon(\bar{x})) - d_2)^2 d\bar{x}. \tag{3.1}$$

A shape prior image S, a given image I, and Ω as a domain are given and λ is a positive parameter balancing the influences from two terms in the model. d_1 and d_2 are average intensity values of $I(\Upsilon)$ in $\{S\}$ and $\{1 - S\}$ respectively. In our numerical experiments, only rigid transformation is considered, but the model can be generalized to non-rigid deformation as well. Therefore the rigid transformation vector $\Upsilon(\bar{x}) = \mu R\bar{x} + T$, where μ is a scaling, R is a rotation matrix with respect to an angle θ, and T is a translation.

For each $\bar{x} \in \Omega$, the first term is forcing $I(\Upsilon(\bar{x}))$ to be close to d_1 using prior shape information $S(\bar{x})$. In a similar way, the second term is compelling $I(\Upsilon(\bar{x}))$ to be close to d_2 utilizing prior shape information $\{1 - S(\bar{x})\}$. After minimizing these three terms, the best Υ, d_1, and d_2 are obtained. The Equation (3.1) is similar to [4], but is different by using the prior shape information S and the rigid transformation Υ. During the image segmentation process, the shape knowledge information supports the robustness to loss of information and image noise and the rigid transformation Υ helps to find the correct correspondence to the transformed image.

3.1 Euler-Lagrange Equations of the Proposed Model

The evolution equations associated with the Euler-Lagrange equations in Equation (3.1) are

$$\frac{\partial \mu}{\partial t} = -\int_\Omega S(\bar{x})(I(\Upsilon(\bar{x})) - d_1)(\nabla I(\Upsilon(\bar{x})))R\bar{x}d\bar{x} -$$
$$\lambda \int_\Omega (1 - S(\bar{x}))(I(\Upsilon(\bar{x})) - d_2)(\nabla I(\Upsilon(\bar{x})))R\bar{x}d\bar{x}, \tag{3.2}$$
$$\frac{\partial \theta}{\partial t} = -\int_\Omega S(\bar{x})(I(\Upsilon(\bar{x})) - d_1)(\nabla I(\Upsilon(\bar{x})))\mu \frac{dR}{d\theta}\bar{x}d\bar{x} -$$
$$\lambda \int_\Omega (1 - S(\bar{x}))(I(\Upsilon(\bar{x})) - d_2)(\nabla I(\Upsilon(\bar{x})))\mu \frac{dR}{d\theta}\bar{x}d\bar{x}, \tag{3.3}$$

$$\frac{\partial T}{\partial t} = -\int_{\Omega} S(\bar{x})(I(\Upsilon(\bar{x})) - d_1)(\nabla I(\Upsilon(\bar{x})))d\bar{x} -$$

$$\lambda \int_{\Omega} (1 - S(\bar{x}))(I(\Upsilon(\bar{x})) - d_2)(\nabla I(\Upsilon(\bar{x})))d\bar{x}, \tag{3.4}$$

$$\frac{\partial d_1}{\partial t} = \int_{\Omega} S(\bar{x})(I(\Upsilon(\bar{x})) - d_1)d\bar{x}, \tag{3.5}$$

$$\frac{\partial d_2}{\partial t} = \lambda \int_{\Omega} (1 - S(\bar{x}))(I(\Upsilon(\bar{x})) - d_2)d\bar{x}, \tag{3.6}$$

where R is the rotation matrix in terms of the angle θ.

3.2 Numerical Results

The Equation (3.1) was solved by finding a steady state solution of the evolution equations. The evolution equations are associated with the Euler-Lagrange equations of the Equation (3.1). A finite difference scheme and the gradient descent method is applied to discretize the evolving equations. Initial value of d_1 and d_2 are 0.95 and 0.01 respectively. Here $\lambda = 1$ is used in the numerical experiments. Figure 7 showed original image, the binary image S as a prior shape information, and synthetic image I with noise, rotation, and loss of information. The numerical results of the proposed model using the prior shape information are shown in Figure 8. In Figure 8, the first one is the binary image as prior shape information and the second one is the given image I. The segmented image and segmented contour result by using the Equation (3.1) are the third and fourth figure in Figure 8. The first figure in Figure 9 and Figure 10 is the given image I. The second and the third figure in Figure 9 showed the numerical results of segmented contour by [4] and the Equation (2.1) to a given Image I. Due to the noise, rotation, and loss of information, only using the model by [4] or the Equation (2.1) was not sufficient to get desired segmentation results. Hence the prior shape information is necessary in the segmentation process. The fourth image in Figure 9 is the segmented contour result using the Equation (3.1). In Figure 10, the second and the third figure showed the numerical results of segmented image by [4] and the Equation (2.1) to a given Image I. The fourth image in Figure 10 is the segmented image result using the Equation (3.1) with a contour as a solid line. The optimal solution μ, R associated with θ, and T from the Equation (3.1) is applied to the Prior Shape Information S to get the segmented image and segmented contour as a solid line from Figure 8 to Figure 10.

4 Conclusions and Future Work

Two new region based variational partial differential equation (PDE) models for an image segmentation are proposed with an application to synthetic and simulated human brain MR images. The first model utilizes a modified piecewise constant Mumford-Shah model. Even though this model performs better than existing model with fuzzy

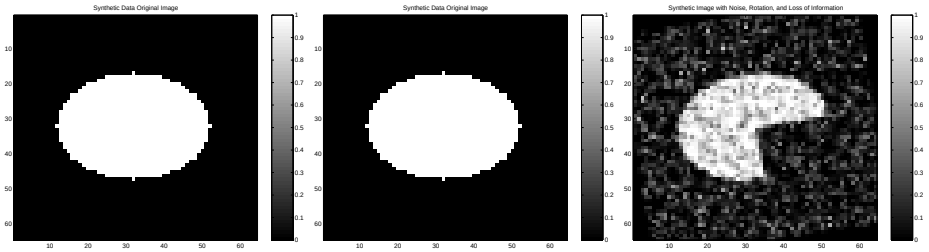

Fig. 7. Left: Original Image, Middle : A Binary Image S as a Prior Shape Information, Right : Given Synthetic Image I with Noise, Loss of Information, and Rotation

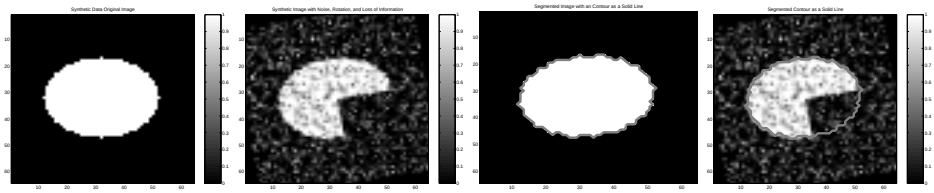

Fig. 8. First : A Binary Image S as a Prior Shape Information, Second: Given Synthetic Image I, Third : Segmented Image with a contour as a Solid Line, Fourth : Given Image I with Segmented Contour as a Solid Line

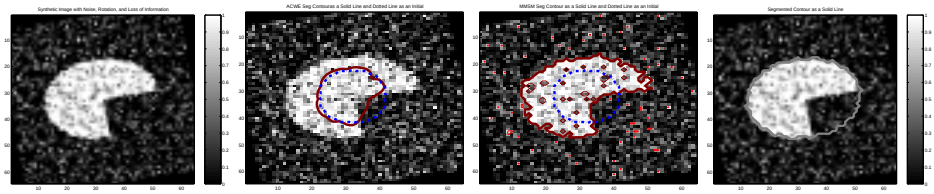

Fig. 9. First : A Given Image I, Second : Segmented Image using an Active Contour without Edges with Dotted Line as Initial Contour and Solid Line as Segmented Contour, Third : Segmented Image using our Proposed Model in Section 2 with Dotted Line as Initial Contour and Solid Line as Segmented Contour, Fourth : Segmented Image using the Prior Shape Information S with Solid Line Contour

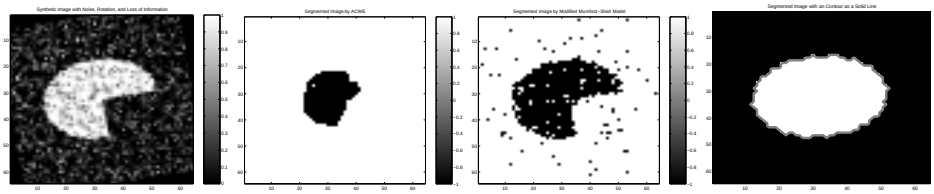

Fig. 10. First : A Given Image I, Second : Segmented Synthetic Image by an Active Contour without Edges, Third : Segmented Synthetic Image by our Proposed Model in Section 2, Fourth : Segmented Synthetic Image with a Solid Line Contour using the Prior Shape Information

images, this algorithm has some limits with strong noise, rotation, and loss of information. Therefore, the second model is obtained using a prior shape information and region intensity value. Numerical Results show the effectiveness and robustness of the presented model against to noise, rotation, loss of information, and artifact. In the future work, the research will be focused on the improvements of the first model with the robustness to the choice of the initial contour. In addition, the generalization of the second model to non-rigid deformation will be developed and the numerical experiments on simulated human brain MR images of the second proposed model will be performed.

Acknowledgement Chen is partially supported by NSF CCF-0527967 and NIH R01 NS052831-01 A1.

References

1. Ambrosio, L. and Tortorelli, V. : Approximation of functionals depending on jumps by elliptic functionals via Γ-convergence . Comm. on Pure and Applied Math. Vol. **43** (1990) 999–1036
2. Baldo, S. : Minimal interface criterion for phase transitions in mixtures of Cahn-Hilliard fluids. Annals. Inst. Henri Poincare. Vol. **7** (1990)67–90
3. Bresson, X., Vandergheynst, P., and Thiran, J. : A variational model for object segmentation using boundary information and shape prior driven by the Mumford-Shah functional Int. J. Comp. Vis. Vol. **68**(2) (2006) 145–162
4. Chan, T. and Vese, L. : Active contours without edges. IEEE Trans. Image Proc. **10** (2) (2001) 266–277
5. Chan, T. and Vese, L. : A level set algorithm for minimizing the Mumford-Shah functional in image processing. Proc. 1st IEEE Workshop Varia. Level Set Meth. Comp. Vis. **13** Vancouver B.C. Canada (2001) 161–168
6. Chen, Y., Tagare, H., Thiruvenkadam, S., Huang, F., Wilson, D., Gopinath, K., Briggs, R., and Geiser, E. : Using prior shapes in geometric active contours in a variational framework. Int. J. Comp. Vis. Vol. **50** (3) (2002) 315–328
7. Cremers, D., Kohlberger, T., and Schnörr, C. : Shpe statistics in kernel space for variational image segmentation. Patt. Recog. 36 (2003) 1929–1943
8. Esedoglu, S. and Tsai, R. : Threshold dynamics for the piecewise constant Mumford-Shah fuctional. CAM Report 04-63 UCLA (2004)
9. Gibou, F., and Fedkiw, R. : A fast hybrid k-means level set algorithm for segmenttion. Stanford Technical Report (2002)

10. Huang, X., Li, Z., and Metaxas, D. : Learning Coupled Prior Shape and Appearance Models for Segmentation. Proc. 7th. Ann. Int. Conf. on Med. Image Comp. Computer-Assi. Interv. MICCAI04 Vol. **I** LNCS-3216 (2004) 60-69.
11. Huang, X., Metaxas, D., and Chen, T. : MetaMorphs: Deformable Shape and Texture Models. Proc. IEEE Comp. Soc. Conf. Comp. Vis. Pat. Recog. CVPR04, Vol. **I** (2004) 496–503
12. Leventon, M., Grimson, E., and Faugeras, O. : Statistical Shape Influence in Geodesic Active Contours. Proc. IEEE Conf. CVPR (2000) 316–323
13. Lie, J., Lysaker, M., and Tai, X. : A binary level set model and some aplications to Mumford-Shah segmentation. CAM Report. Vol. **31** (2004)
14. Modica, L. : The gradient theory of phase transitions and the minimal interface criterion. Arch. Rational Mech. Anal. Vol. **98** (1987) 123–142
15. Mumford, D. and Shah, J. : Optimal approximations by piecewise smooth functions and associated variational problems. Comm. on Pure and Applied Math. Vol. **42** (1989) 577–685
16. Osher, S. and Fedkiw, R. : Level set methods and dynamic implicit surfaces. Springer Verlag, New York, (2003)
17. Rousson, M. Paragios, N.: Shape prior for level set representations. Comp. Vis. ECCV2002 7th. Eur. Conf. Comp. Vis. Copenhgen Demark Proc. (2002) 78–92
18. Shen. J.: Γ-Convergence Approximation to Piecewise Constant Mumford-Shah Segmentation. Lec. Notes Comp. Sci., 3708 (2005) 499–506
19. Shen. J.: A stochastic-variational model for soft Mumford-Shah segmentation . Int. J. Biomed. Imaging, special issue on "Recent Advances in Mathematical Methods for the Processing of Biomedical Images," Vol. **2006** (2006) 1–14
20. Wang, M. and Zhou, S. : Phase Field: A Variational Method for Structural Topology Optimization . Computer Modeling in Engineering & Sciences. Vol. **6** no.6 (2004) 547–566